Cutaneous Wound Healing in Diabetic Mice Is Improved by Topical Mineralocorticoid Receptor Blockade

Van Tuan Nguyen[1,2,3], Nicolette Farman[1], Roberto Palacios-Ramirez[1], Maria Sbeih[2], Francine Behar-Cohen[1,4], Sélim Aractingi[2,4,5,7] and Frederic Jaisser[1,6,7]

Skin ulcers resulting from impaired wound healing are a serious complication of diabetes. Unresolved inflammation, associated with the dysregulation of both the phenotype and function of macrophages, is involved in the poor healing of diabetic wounds. Here, we report that topical pharmacological inhibition of the mineralocorticoid receptor (MR) by canrenoate or MR small interfering RNA can resolve inflammation to improve delayed skin wound healing in diabetic mouse models; importantly, wounds from normal mice are unaffected. The beneficial effect of canrenoate is associated with an increased ratio of anti-inflammatory M2 macrophages to proinflammatory M1 macrophages in diabetic wounds. Furthermore, we show that MR blockade leads to downregulation of the MR target, LCN2, which may facilitate macrophage polarization toward the M2 phenotype and improve impaired angiogenesis in diabetic wounds. Indeed, diabetic LCN2-deficient mice showed improved wound healing associated with macrophage M2 polarization and angiogenesis. In addition, recombinant LCN2 protein prevented IL-4–induced macrophage switch from M1 to M2 phenotype. In conclusion, topical MR blockade accelerates skin wound healing in diabetic mice via LCN2 reduction, M2 macrophage polarization, prevention of inflammation, and induction of angiogenesis.

Journal of Investigative Dermatology (2020) **140,** 223–234; doi:10.1016/j.jid.2019.04.030

INTRODUCTION

Impaired cutaneous wound healing, responsible for chronic ulcers, represents one of the most important complications of diabetes. Indeed, the incidence of diabetic foot ulcers is increasing because of the high prevalence of diabetes mellitus worldwide and the longer life expectancy of patients (Boulton et al., 2005). The prevalence of global diabetic foot ulcers was recently reported to be 6.3% and up to 13.0% in North America (Zhang et al., 2017). Ulcers remain in a chronic inflammation state that prevents them from healing, resulting in other severe complications such as pain, infection, and eventually amputation (Greenhalgh, 2003; Noor et al., 2017; Peters and Lipsky, 2013). Previous studies showed that most diabetic amputations are preceded by a foot ulceration, which subsequently results in serious gangrene or infection (Boulton et al., 2005; Lepantalo et al., 2011). Diabetic foot ulcers are thus a major health issue that significantly affects the lives of patients, resulting in a high financial burden in many countries (Boulton et al., 2005). The prevention and appropriate care of diabetic ulcers are thus of major importance.

Several therapies have been proposed for diabetic ulcers but effective treatment is still needed (Clokie et al., 2017; Dinh et al., 2012; Galiano et al., 2004). The lack of therapeutic tools likely results from the complex mechanisms involved in the development of unhealed wounds. Many pathogenic factors, such as vascular defects and neuropathy, are responsible for diabetic ulcers (Ahmed and Antonsen, 2016; Boulton, 2014; Brem and Tomic-Canic, 2007; Dinh et al., 2012). A chronic inflammatory environment is also a common feature observed in unhealed wounds and is mainly associated with the uncontrolled recruitment and activation of inflammatory cells, in particular monocytes and macrophages (Boniakowski et al., 2017; Leal et al., 2015; Okizaki et al., 2015).

During the wound repair process, macrophages present various phenotypes and functions, depending on the stage of the healing response and how they are activated. During the early phase of wound healing, classically activated macrophages, known as M1 macrophages, are recruited and secrete proinflammatory cytokines to kill pathogens and clear away the damaged tissue. In contrast, alternatively activated M2 macrophages secrete anti-inflammatory factors to resolve inflammation and produce factors required for later regenerative phases. The balance between these macrophage subpopulations is pivotal for maintaining a physiological healing process (Gordon, 2003; Mahdavian Delavary et al.,

[1]*INSERM, Centre de Recherche des Cordeliers, Sorbonne Université, USPC, Université Paris Descartes, Université Paris Diderot, Paris, France;* [2]*Laboratory of progenitors and endothelial cells during and after pregnancy, INSERM UMR 938, Centre de Recherche St Antoine, Sorbonne Université, Paris, France;* [3]*Department of Basic Science, Thai Nguyen University of Agriculture and Forestry, Thainguyen, Vietnam;* [4]*Faculty of Medicine, Université Paris Descartes, Paris, France;* [5]*Department of Dermatology, Hôpital Cochin-Tarnier, Paris, France; and* [6]*INSERM, Clinical Investigation Centre 1433, Vandoeuvre-lès-Nancy, France*

[7]*These authors contributed equally to this work.*

Correspondence: Frederic Jaisser, MD, PhD, UMR 1138, INSERM, Centre de Recherche des Cordeliers, 15 rue de l'Ecole de Médecine, 75006 Paris, France. E-mail: frederic.jaisser@inserm.fr

Abbreviations: CT, control; GC, glucocorticoid; KO, knockout; MR, mineralocorticoid receptor; siRNA, small interfering RNA; STZ, streptozotocin

Received 29 August 2018; revised 20 March 2019; accepted 8 April 2019; accepted manuscript published online 3 July 2019; corrected proof published online 6 September 2019

2011; Mantovani et al., 2004). However, in unhealed wounds, such as diabetic ulcers, macrophages are chronically activated and restrained to the M1 phenotype, heavily contributing to the chronic inflammatory microenvironment observed in these wounds. Moreover, such prolonged inflammation delays the process of tissue regeneration, including re-epithelialization, granulation tissue formation, and vascularization (Boniakowski et al., 2017; He et al., 2017; Maruyama et al., 2007; Okizaki et al., 2015). Enhancing macrophage polarization toward the M2 phenotype may help to promote cellular proliferation and angiogenesis and to accelerate diabetic wound closure (He et al., 2017; Leal et al., 2015; Okizaki et al., 2015).

The mineralocorticoid receptor (MR), a steroid receptor that belongs to the nuclear receptor superfamily of transcription factors, plays a key role in various physiological and pathophysiological phenomena, including obesity- and diabetes-related complications, such as vascular dysfunction, insulin resistance, metabolic disorders, and chronic inflammation (Guo et al., 2008; Hirata et al., 2009; Jaisser and Farman, 2015). We recently reported the involvement of MR activation in delayed wound closure in type 1 diabetes and the improvement of impaired wound re-epithelialization following local application of an MR antagonist to the wounds (Nguyen et al., 2016). However, we did not explore the integrated impact on either the epidermis or dermis in diabetic wounds or the underlying mechanisms of the benefit of local MR antagonism. It is not known whether MR acts on the inflammatory response and dermal angiogenesis during wound repair in diabetes. Here, we analyzed the positive impact of topical pharmacological MR blockade on impaired wound healing of streptozotocin (STZ)-treated mice and of db-db mice, a model of type 2 diabetes. We focused on inflammation and angiogenesis and identified LCN2, a primary MR target (Buonafine et al., 2018; Martínez-Martínez et al., 2017), as a potential mechanism involved in these beneficial effects.

RESULTS

MR blockade rescues delayed cutaneous wound closure in diabetic mice

We have shown previously that local MR blockade with canrenoate improves the delayed wound re-epithelialization of type 1 diabetic mice (STZ mice) (Nguyen et al., 2016). To exclude MR-independent effects of canrenoate, we designed an in vivo experimental strategy to interfere specifically with the MR. Topical treatment with MR small interfering RNA (siRNA) blocked MR upregulation in STZ wounds (Supplementary Figure S1a) and restored the defective re-epithelialization of STZ mice, as compared with those of diabetic mice treated by scrambled siRNA (Supplementary Figure S1c–g). These results are quite comparable to those previously obtained using canrenoate, indicating that MR antagonism and silencing is beneficial for wounding in type 1 diabetic mice.

Next, we questioned the effect of canrenoate on the delayed wound healing of type 2 diabetes using db-db mice, a genetic mouse model of type 2 diabetes. MR mRNA expression was higher in wounded skin and the surrounding normal skin of db-db mice than that of normal db/$^{+}$ control (CT) mice (Figure 1a), raising the question of the role of MR overexpression in abnormal wound repair in type 2 diabetes. Wound healing was strongly impaired in db-db mice relative to that of CT mice (Figure 1b and c). Consistent with our observations in STZ mice, local treatment with canrenoate improved the wound healing delay in db-db mice, whereas it did not modify wound closure in normal CT mice (Figure 1b and c). Moreover, keratin-14 staining showed that impaired re-epithelialization of db-db wounds was rescued by local canrenoate treatment, as illustrated by the longer neoepidermis at the edges of the wound sections (Figure 1d and e) and the shorter residual wound length (the distance between two edges) in canrenoate-treated db-db mice than in phosphate buffered saline–treated db-db mice (Figure 1d and f). This reduction in wound surface is indicative of re-epithelialization rather than wound contraction. The improvement of re-epithelialization was accompanied by a higher number of proliferating Ki67-positive keratinocytes in the neoepidermis of the wounds of canrenoate-treated than phosphate buffered saline–treated db-db mice (Figure 1g and h). These observations suggest that the effects of topical canrenoate treatment on diabetic wound healing are mediated by MR signaling. Thus, topical MR blockade restored the impaired proliferation of epidermal keratinocytes and blunted the delayed re-epithelialization of wounds in 2 diabetes mouse models. In contrast, these phenomena were not found in wounds of normal CT mice.

Impaired wound angiogenesis in diabetic mice is improved by MR antagonism

Impaired dermal wound angiogenesis is a key contributor to the wound healing defect of diabetes. Herein, we explored the role of MR in the defective wound angiogenesis of diabetic mouse models. The density of CD31^{+} blood vessels was lower in the wounds of STZ-induced (Figure 2a in red, 2b) and db-db diabetic mice than those of CT mice (Figure 2e and f), consistent with previous reports. Decreased vessel density of diabetic wounds was partly rescued by topical treatment of these wounds with canrenoate (Figure 2a, b, e, and f). MR inactivation by local MR siRNA treatment of STZ wounds also showed a beneficial effect on wound angiogenesis (Supplementary Figure S1h and i). The improvement of vessel density in canrenoate-treated diabetic wounds was associated with an increased number of CD45^{-}CD31^{+} endothelial cells in the wound beds, as quantified by FACS analysis of wound specimens (Figure 2c, d, g, and h). Moreover, by quantification of CD31^{+}Ki67^{+} double positive cells on wound sections of STZ mice (Figure 2a, red and green), we found fewer proliferating endothelial cells in STZ wounds than in controls (2.87% ± 1.08, $n = 7$ vs 7.18% ± 0.71, $n = 7$, respectively), and this decrease was rescued by canrenoate treatment (STZ + phosphate buffered saline: 2.87% ± 1.08, $n = 7$ vs STZ + canrenoate: 6.37% ± 1.2, $n = 7$). These observations suggest that the activation of MR in the skin of diabetic mice is involved in the impaired wound angiogenesis of these animals, and that MR blockade could prevent such defects through increased proliferation of endothelial cells forming novel microvessels in wounds.

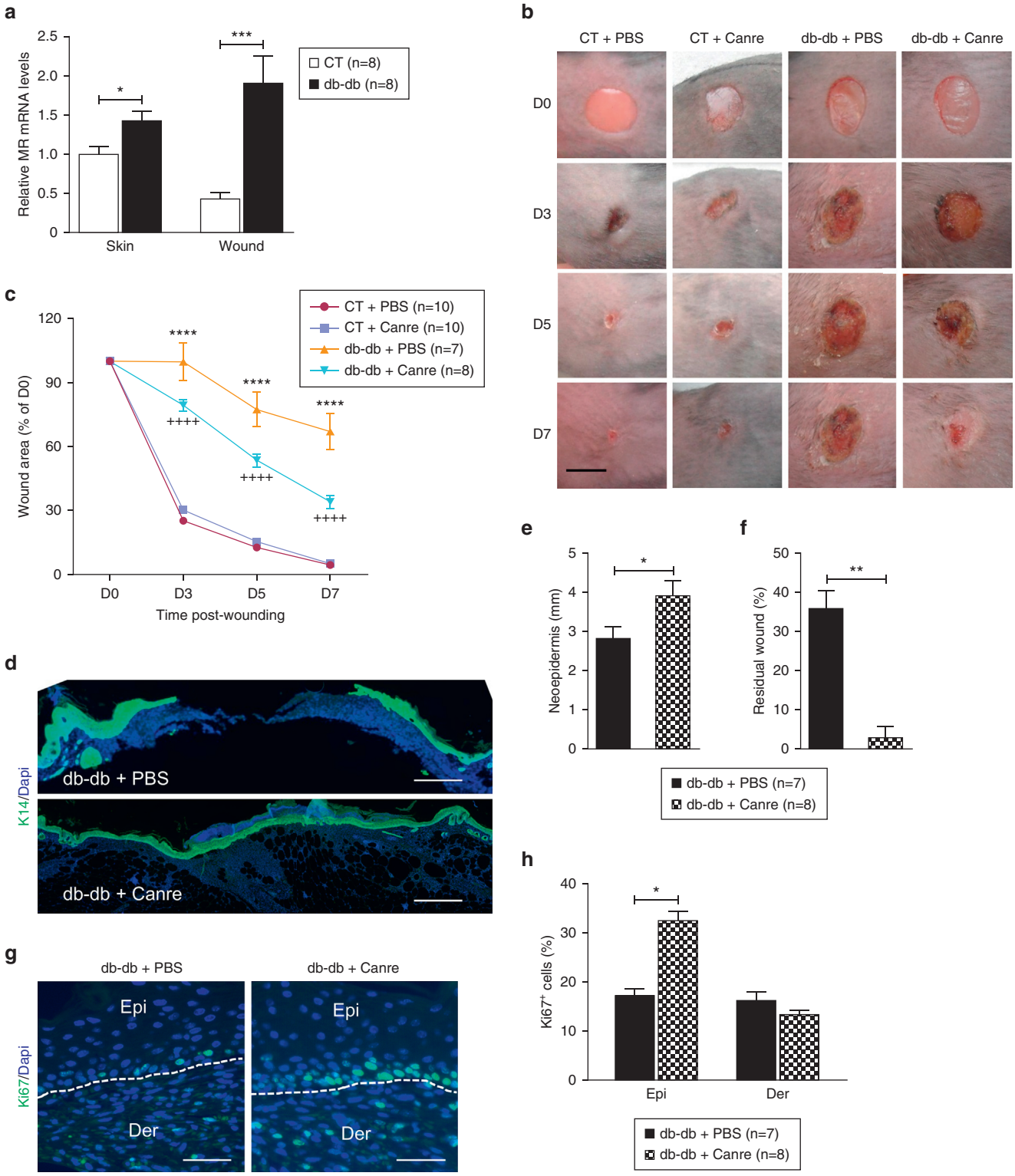

Figure 1. Canrenoate improves delayed wound healing in type 2 diabetic mice. (**a**) Real-time PCR analysis of MR mRNA expression in the skin or wounds (day 7) of db-db mice, relative to that of CT. (**b**) Photographs and (**c**) quantification of the wound area of CT and db-db mice treated with canrenoate or PBS at the indicated time post-wounding. (**d**) Wound sections at day 7 post-wounding labeled with anti-K14 antibody (green) and DAPI (blue). Quantification of (**e**) the length of the neoepidermis and (**f**) diameter of the residual wound. (**g**) Anti-Ki67 (green) staining and quantification of Ki67-positive cells in the neoepidermis and (**h**) underlying dermis; dotted lines represent the dermo-epidermis junction. Data represent mean ± SEM; n = number of mice per group, from 2 experimental series. (a, e, f, and h) Mann-Whitney test; c: two-way ANOVA followed by the Newman-Keuls multiple comparison test. *$P < 0.05$; **$P < 0.01$; ***$P < 0.001$; ****$P < 0.0001$ db-db vs CT; $^{++++}P < 0.0001$ db-db vs db-db + Canre. ANOVA, analysis of variance; Canre, canrenoate; CT, control; Der, dermis; Epi, neoepidermis; MR, mineralocorticoid receptor; PBS, phosphate buffered saline; SEM, standard error of the mean. (d) Bar = 500 μm, (g) Bar = 100 μm.

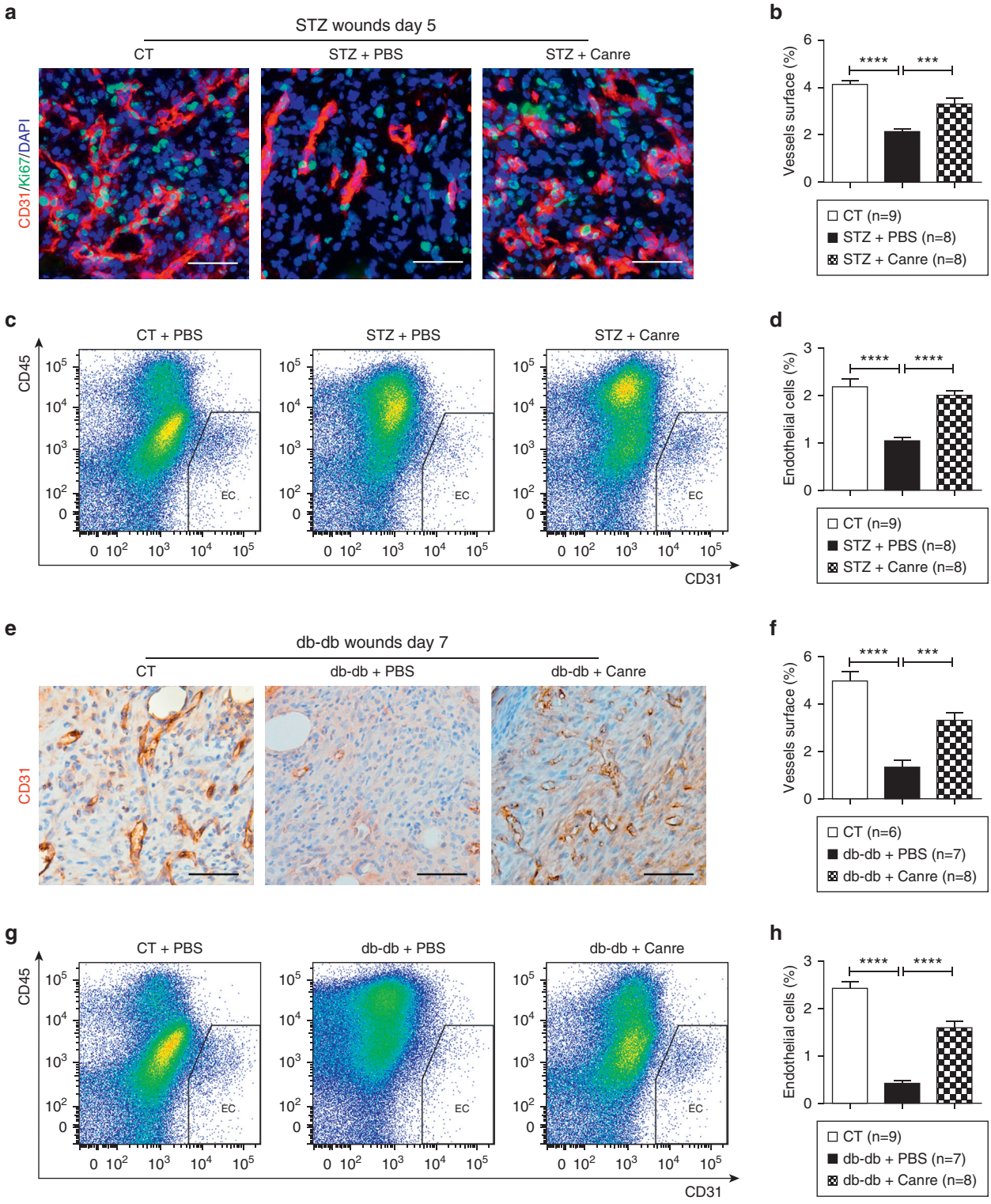

Figure 2. Canrenoate improves impaired wound angiogenesis in diabetic mice. (**a**) Photographs of wound sections doubled-stained for CD31 (red) and Ki67 (green), showing neomicrovessels formed in wound beds of STZ mice and (**e**) stained with CD31 only in db-db mice. (**b**) Quantification of $CD31^+$ microvessels in wound of STZ and (**f**) db-db mice after treatment with Canre or PBS. (**c, g**) Dot plot of FACS analysis of wound cells for the quantification of $CD45^-CD31^+$ (**d**) endothelial cells in wound of STZ and of (**h**) db-db mice after treatment with Canre or PBS. Data represent mean ± SEM; n = number of mice per group, from 3 (STZ) and 2 (db-db) experimental series. One-way ANOVA followed by the Newman-Keuls multiple comparison test. $^{***}P < 0.001$; $^{****}P < 0.0001$. ANOVA, analysis of variance; Canre, canrenoate; CT, control; FACS, fluorescence activated cell sorting; PBS, phosphate buffered saline; SEM, standard error of the mean; STZ, streptozotocin. Bar = 100 μm.

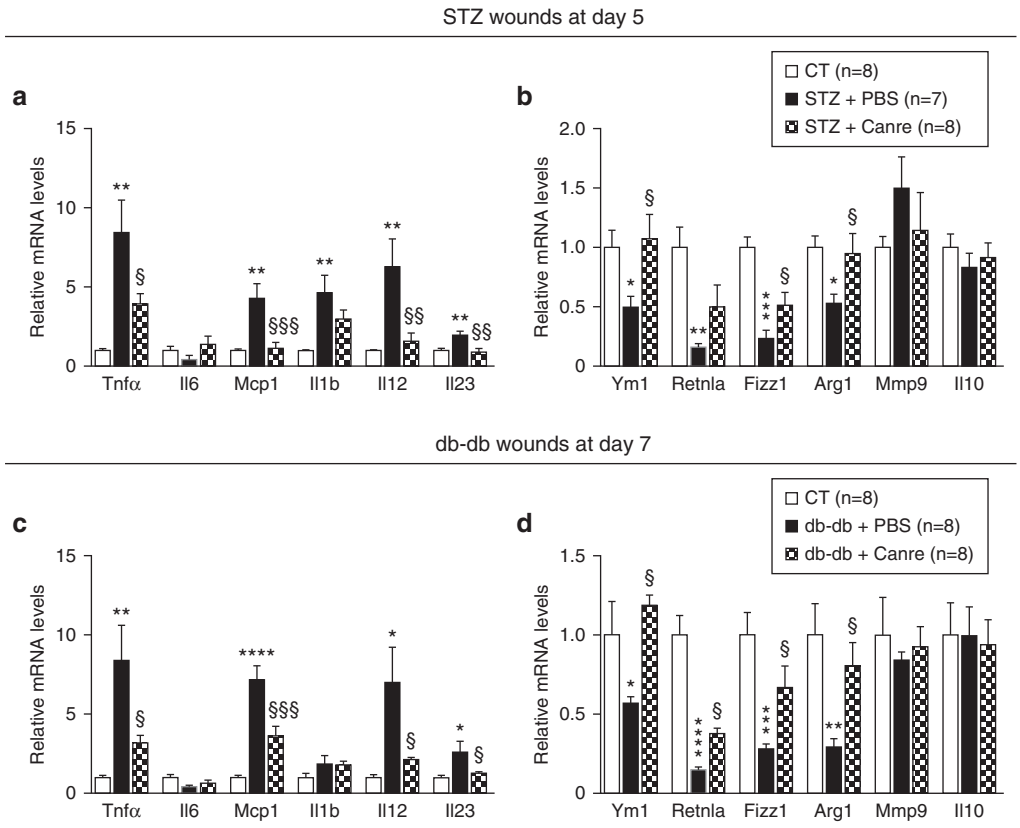

Figure 3. Canrenoate regulates the wound production of pro- and anti-inflammatory factors. Total RNA was extracted from wounded skin of CT, STZ (day 5 post-wounding), or db-db (day 7 post-wounding) mice. Cytokine mRNA levels were analyzed by quantitative RT-PCR. Proinflammatory cytokine mRNA levels in (**a**) STZ and (**c**) db-db wounds treated with Canre or PBS, relative to those of CT wounds treated with PBS. Anti-inflammatory cytokines mRNA levels in (**b**) STZ and (**d**) db-db wounds treated with Canre or PBS, relative to those of CT wounds treated with PBS. Data represent mean ± SEM; n = number of mice per group, from 2 experimental series. One-way ANOVA followed by the Newman-Keuls multiple comparison test. $^{*}P < 0.05$; $^{**}P < 0.01$; $^{***}P < 0.001$; $^{****}P < 0.0001$ STZ or db-db vs CT; $^{§}P < 0.05$; $^{§§}P < 0.01$; $^{§§§}P < 0.001$ STZ vs STZ + Canre (a and b) or db-db vs db-db + Canre (c and d). ANOVA, analysis of variance; Canre, canrenoate; CT, control, PBS, phosphate buffered saline; RT-PCR, reverse transcriptase—PCR; SEM, standard error of the mean; STZ, streptozotocin.

MR blockade ameliorates inflammation of diabetic wounds

Chronic inflammation is a common feature of diabetic ulcers. We examined whether MR plays a role in maintaining inflammation in diabetic wounds by studying the impact of MR blockade on the expression of some pro- and anti-inflammatory markers in wounds (Ashcroft et al., 2012; Barrientos et al., 2008; Ramalho et al., 2018). Local treatment with canrenoate attenuated the overexpression of some proinflammatory genes, such as *Tnfa*, *Mcpt1*, *Il12*, and *Il23*, in diabetic wounds (Figure 3a and c). Consistent with this effect, the repression of anti-inflammatory factors in diabetic wounds was rescued by canrenoate treatment (Figure 3b and d). Thus, MR blockade blunted the inflammation observed in diabetic wounds and resulted in an anti-inflammatory status that could improve the impaired cellular proliferation and poor angiogenesis.

MR antagonism induces the switch of unrestrained M1 toward M2 macrophages in diabetic wounds

A failure to switch from activated M1 macrophages to alternative M2 macrophages leads to chronic inflammation and impaired angiogenesis in various situations of delayed wound healing, including venous leg ulcers and diabetic foot ulcers (Guo et al., 2016; Okizaki et al., 2015; Sindrilaru et al., 2011). We investigated whether the beneficial effect of canrenoate treatment was associated with a switch of activated M1 macrophages toward the alternative M2 macrophage population. Wounds from both STZ and db-db mice showed more M1 macrophages ($Ly6C^{hi}$) associated with fewer M2 macrophages ($Ly6C^{low}$) than CT mice, whereas the total number of macrophages in diabetic wounds was not different from that in control wounds (Figure 4). These observations are consistent with a number of previous reports showing the accumulation and persistence of activated M1 macrophages in diabetic wounds (Guo et al., 2016; Leal et al., 2015; Okizaki et al., 2015). Importantly, the polarization of diabetic-wound macrophages was nearly restored to the levels of CT mice by topical canrenoate treatment. Canrenoate blunted the increase in M1 macrophages in STZ and db-db wounds (Figure 4a, c, e, and g) and the associated decrease in M2 macrophages (Figure 4a, d, e, and h). MR blockade also blunted overexpression of the proinflammatory marker Ly6C by diabetic-wound macrophages (Supplementary Figure S2a and b). These results suggest that topical MR blockade promotes a shift of proinflammatory M1 macrophages toward the anti-inflammatory M2 phenotype to resolve inflammation, promote angiogenesis, and accelerate wound healing.

MR blockade rescues the impaired macrophage expression of angiogenic factors in diabetic wounds

In addition to their pathogen-killing activity, macrophages in wounds also promote cellular proliferation and tissue regeneration, including re-epithelialization and dermal vascularization (Gordon, 2003; Lucas et al., 2010). We tested whether canrenoate treatment improves delayed diabetic wound angiogenesis through the modulation of macrophage polarization by assessing a panel of proangiogenic factors in wound tissue. Five days after wounding, gene expression of proangiogenic factors was impaired in STZ wounds with a significant decrease of *Fgf2*, *Plgf*, *Tie2*, and *Angpt2* mRNA levels (Figure 5a). Importantly, topical

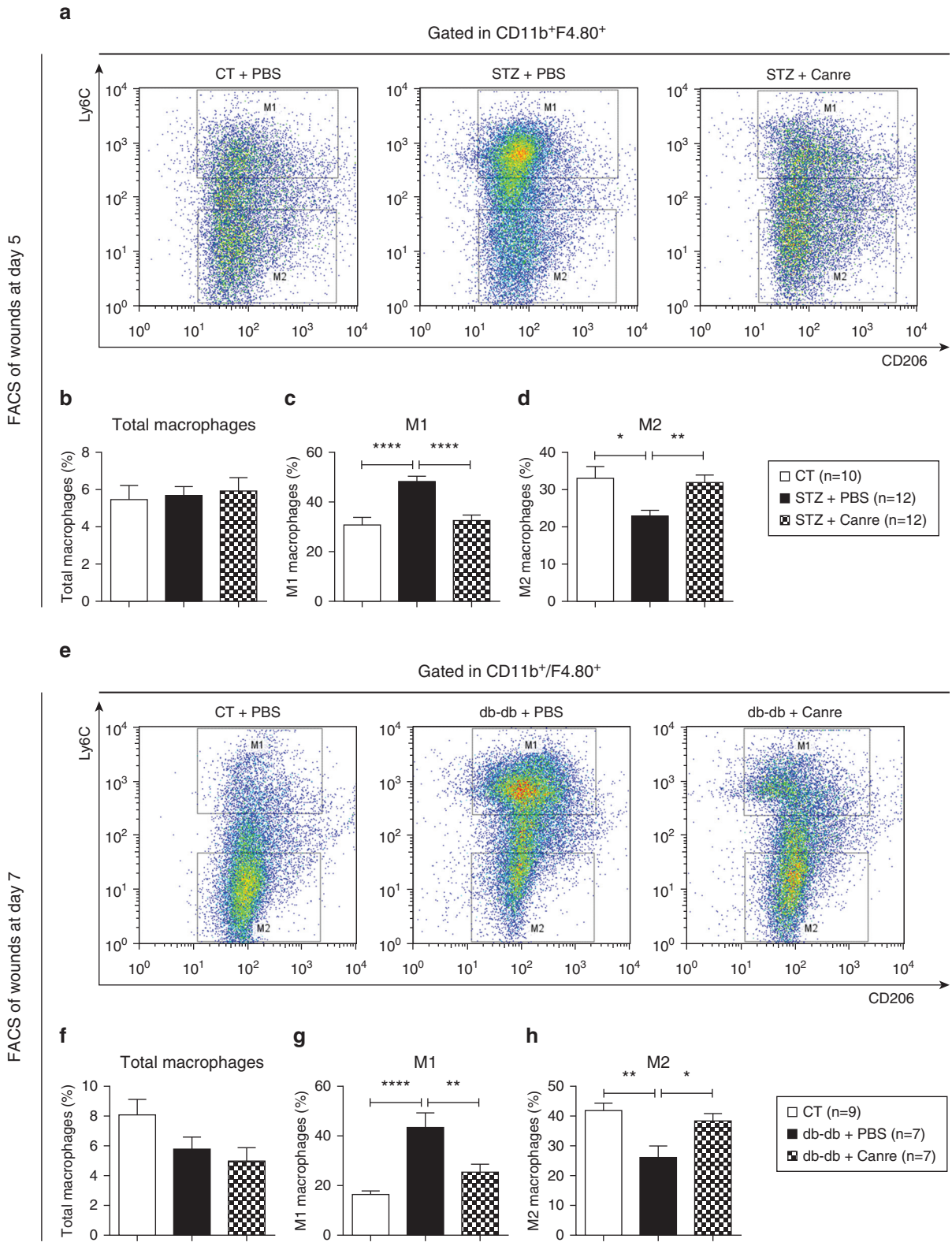

Figure 4. Canrenoate enhances unrestrained polarization of M1 to M2 macrophages. Wounded skin specimens were collected after five (for STZ mice) or seven days (for db-db mice) of treatment with Canre or PBS. (**a, e**) Dot plot of FACS analysis of wound cells for the quantification of (**c**, **g**) $CD11b^{+}F4.80^{+}Ly6C^{hi}$ M1 macrophages and (**d**, **h**) $CD11b^{+}F4.80^{+}Ly6C^{low}$ M2 macrophages in wounds of (c, d) STZ and (g, h) db-db mice after treatment with Canre or PBS, as the percentage of (**b**, **f**) total $CD11b^{+}F4.80^{+}$ macrophages. Data represent mean ± SEM; n = number of mice per group, from 3 (STZ) and 2 (db-db) experimental series. One-way ANOVA followed by the Newman-Keuls multiple comparison test. $^{*}P < 0.05$; $^{**}P < 0.01$; $^{****}P < 0.0001$. ANOVA, analysis of variance; Canre, canrenoate; CT, control, PBS, phosphate buffered saline; SEM, standard error of the mean; STZ, streptozotocin.

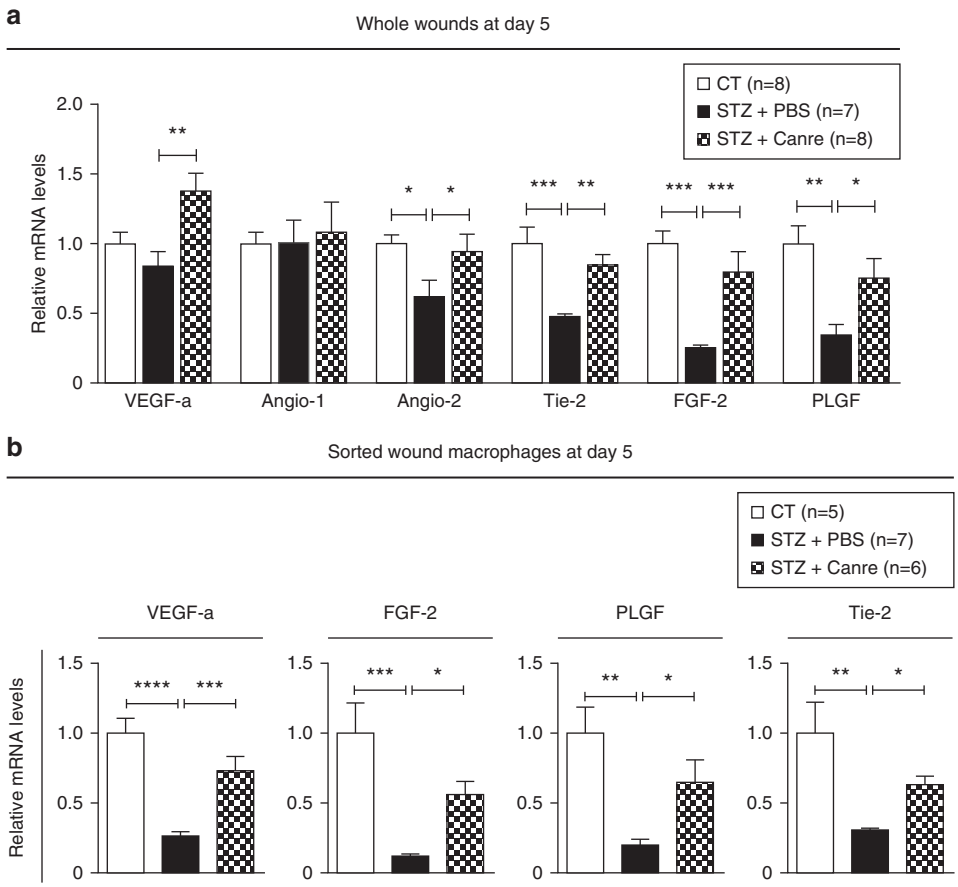

Figure 5. Canrenoate induces macrophage expression of angiogenic factors. Wounded skin specimens from CT or STZ mice were collected five days of treatment with Canre or PBS. Total RNA extracted from whole tissue or sorted macrophages was used to analyze proangiogenic factors. (**a**) Proangiogenic mRNA levels in whole wounded skin from STZ mice treated with Canre or PBS, relative to those of CT wounds treated with PBS. (**b**) Proangiogenic mRNA levels in total macrophages isolated from wounded skin of STZ mice treated with Canre or PBS, relative to those of CT wounds treated with PBS. Data represent mean ± SEM; n = number of mice per group, from 2 experimental series. One-way ANOVA followed by the Newman-Keuls multiple comparison test. $^{*}P < 0.05$; $^{**}P < 0.01$; $^{***}P < 0.001$; $^{****}P < 0.0001$. ANOVA, analysis of variance; Canre, canrenoate; CT, control, PBS, phosphate buffered saline; SEM, standard error of the mean; STZ, streptozotocin.

canrenoate application restored the expression of these factors in diabetic wounds (Figure 5a). We then isolated macrophages ($CD11b^{+}F4.80^{+}Ly6G^{-}$) from wounded skin by FACS to analyze the expression of proangiogenic genes. *Vegfa*, *Fgf2*, *Plgf*, and *Tie2* mRNA levels were significantly lower in macrophages isolated from STZ wounds than those from control wounds, whereas topical application of canrenoate restored the inadequate expression of these angiogenic factors (Figure 5b).

The MR target LCN2 promotes macrophage phenotypic polarization and switching and angiogenesis in diabetic wounds

We recently showed that LCN2 is a primary target of aldosterone and mineralocorticoid receptor signaling in many organs, and that LCN2 plays a key role in the action of mineralocorticoids in the cardiovascular system (Buonafine et al., 2018). LCN2 mRNA and protein expression were much higher in diabetic wounds than in CT nondiabetic wounds (Figure 6a and b; Supplementary Figure S3a and b). Local canrenoate or MR siRNA treatment lowered the upregulated expression of LCN2 in diabetic wounds to near the level found in control wounds, indicating that LCN2 is also an MR target in diabetic skin (Figure 6a and b; Supplementary Figure S1b; Supplementary Figure S3). We assessed whether LCN2 is involved in the impaired healing of diabetic wounds using a global *Lcn2*-knockout (KO) mouse model. Wound closure in diabetic STZ mice was significantly impaired relative to that of CT nondiabetic mice, but LCN2 inactivation prevented the delay in wound healing in *Lcn2*-KO diabetic mice (Figure 6c and d). Of note, LCN2 deficiency did not affect wound healing in normal nondiabetic mice (Figure 6c and d). FACS analysis of wound specimens demonstrated that LCN2 inactivation resulted in M1 to M2 macrophage polarization; the increase of proinflammatory M1 macrophages in CT diabetic wounds was blunted in LCN2-deficient diabetic mice (Figure 6e), whereas the decrease of M2 macrophages in diabetic wounds was prevented (Figure 6f). Importantly, LCN2 deficiency prevented the impaired angiogenesis associated with diabetes, with the presence of more endothelial cells in the wounds of diabetic *Lcn2*-KO mice than those of CT diabetic mice (Figure 6g). Moreover, expression of the proangiogenic genes *Vegfa*, *Fgf2*, *Plgf*, and *Tie2* was higher in STZ *Lcn2*-KO macrophages than in STZ CT mice (Figure 6h).

LCN2 protein induces an unrestrained proinflammatory M1 macrophage phenotype in vitro

We hypothesized that the MR target LCN2 participates in the deleterious effect of MR activation in diabetic wound healing by tipping macrophage functional and phenotypic polarization from proangiogenic M2 macrophages toward proinflammatory M1. Macrophages isolated from the peritoneum of wild-type mice were first pretreated with lipopolysaccharide to induce an M1 phenotype and then with IL-4 to switch them toward an M2 phenotype (Supplementary Figure S4a). FACS analysis showed that treatment with recombinant LCN2

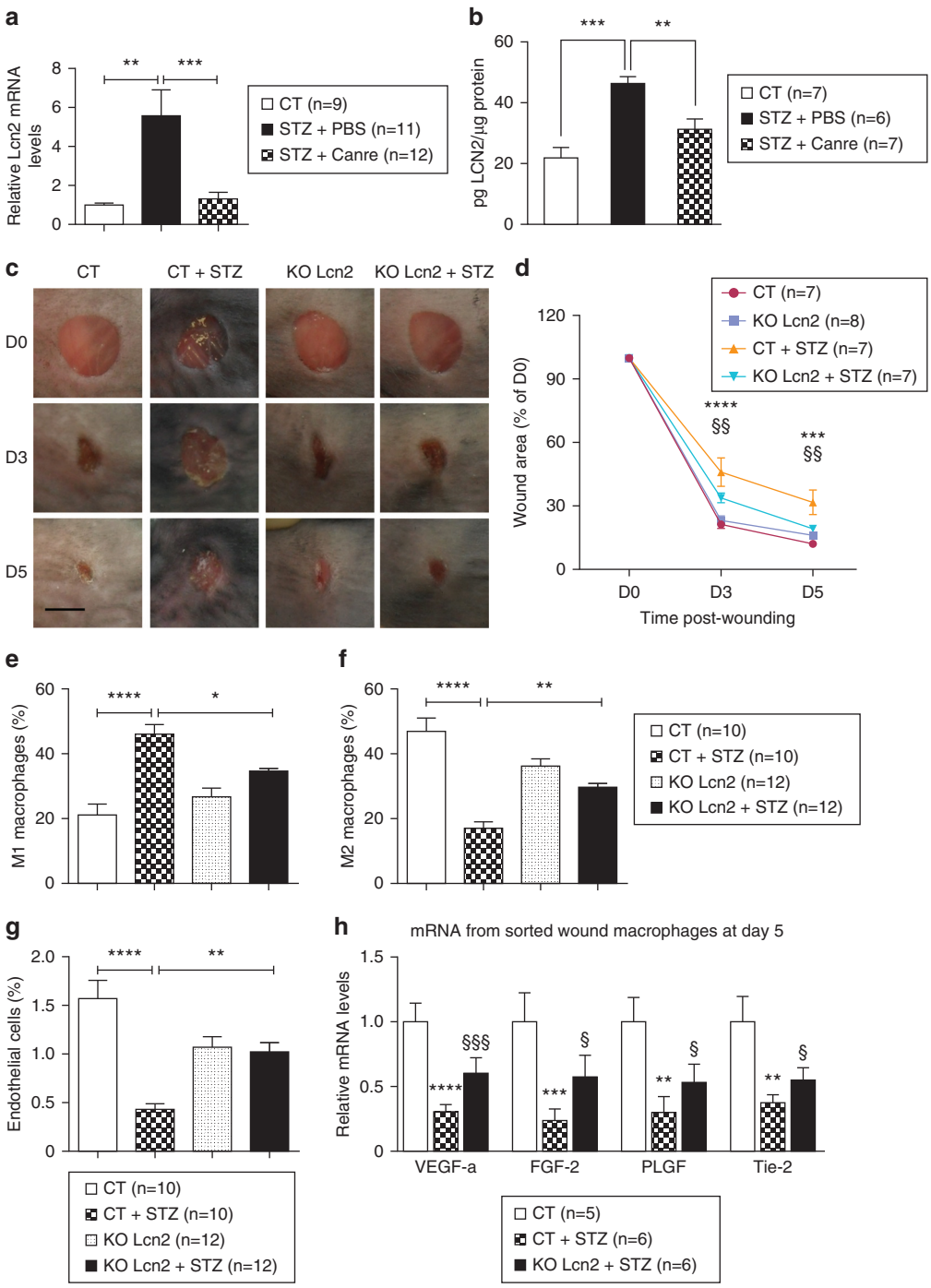

Figure 6. LCN2 deficiency prevents the diabetes-induced delay of wound healing. (**a**) LCN2 mRNA and (**b**) protein levels in wounds at day 5 were analyzed by real-time PCR and ELISA. (**c**–**h**) Diabetes was induced in wild-type (CT) and *Lcn2* KO mice by STZ injections before wounding. (**c**) Photographs and (**d**) quantification of the wound area from CT and *Lcn2* KO mice with or without STZ treatment at the indicated times post-wounding. (**e**) M1 and (**f**) and M2 macrophages and (**g**) endothelial cells of wounds at day 5 were quantified by FACS analysis. (**h**) Total macrophages were sorted from wounded skin at day 5 and angiogenic factors mRNA levels were analyzed by real-time PCR. Data represent mean ± SEM; n = number of mice per group, from 2 experimental series. (a, e–h) one-way ANOVA followed by the Newman-Keuls multiple comparison test; (d) 2-way ANOVA followed by the Newman-Keuls multiple comparison test. $^{*}P < 0.05$; $^{**}P < 0.01$; $^{***}P < 0.001$; $^{****}P < 0.0001$ CT + STZ vs CT. $^{§§}P < 0.01$ CT + STZ vs *Lcn2* KO + STZ. ANOVA, analysis of variance; Canre, canrenoate; CT, control; FACS, fluorescence activated cell sorting; KO, knockout; PBS, phosphate buffered saline; SEM, standard error of the mean; STZ, streptozotocin.

resulted in a higher percentage of Ly6C^{hi} M1 macrophages (Supplementary Figure S4b) together with fewer Ly6C^{low} M2 macrophages (Supplementary Figure S4c), indicating that recombinant LCN2 inhibited the ability of lipopolysaccharide-pretreated macrophages to switch to the M2 phenotype in response to IL-4. This was associated with decreased expression of the angiogenic genes *Vegfa* and *Plgf* (Supplementary Figure S4d and e).

Overall, these data show that MR blockade controls the phenotypic polarization of macrophages toward a repair M2 phenotype and promotes dermal angiogenesis through modulation of the expression and activity of LCN2, thereby improving the delayed wound healing in diabetes (Supplementary Figure S5).

DISCUSSION

By using 2 mouse models of diabetes (STZ-induced type 1 and db-db type 2 diabetic mice), we demonstrate that inflammation and impaired healing of diabetic wounds are associated with the activation of MR signaling. Topical inhibition of this pathway provided a clear benefit to improve healing of these pathological wounds. This effect acts via inducing the polarization of macrophages toward the M2 phenotype, helping to resolve inflammation and rescue the

angiogenesis defect of diabetic wounds. Moreover, we identified the MR target LCN2 as one of the underlying signaling pathways. In contrast, MR blockades do not modify wound closure from normal mice. We propose that inadequate MR occupancy by exogenous glucocorticoid (GC) or locally produced GC, as well as enhanced MR expression, may explain the benefit of MR blockade in a variety of pathological situations such as dermocorticoid treatments, UV irradiation, diabetic delayed wound healing, and perhaps psoriatic skin or GC-treated psoriasis (Hannen et al., 2017; Nguyen et al., 2016; Stojadinovic et al., 2016). In addition, local steroidogenesis and modulation of 11β-hydroxysteroid dehydrogenase type 1 may interfere with MR/GC receptor signaling balance in skin diseases (Sevilla and Pérez, 2018; Slominski et al., 2014, 2015; Tiganescu et al., 2013). Efforts toward better integrations of these factors should help to propose novel therapeutic improvements of delayed wound healing.

During wound healing, macrophages are significantly involved in the repair process (Brancato and Albina, 2011; Lucas et al., 2010; Rahmani et al., 2018). Importantly, they show heterogeneous phenotypes and functions and can switch or polarize between phenotypes to adapt to the wound stage (Boniakowski et al., 2017; Novak and Koh, 2013). The balance of such macrophage populations is pivotal for the progression of wound healing. However, most diabetic wounds do not progress, but remain in a chronic state of inflammation. This mainly results from a defect in the phenotypic switch of macrophages, leading to the sustained presence of proinflammatory M1 macrophages and overproduction of proinflammatory cytokines in wounds (Boniakowski et al., 2017; Leal et al., 2015; Okizaki et al., 2015). Here, we demonstrate that topical inhibition of the MR promotes the polarization of activated M1 macrophages ($CD11b^{+}/F4.80^{+}/Ly6C^{hi}$) in diabetic wounds toward an anti-inflammatory M2 phenotype ($CD11b^{+}/F4.80^{+}/Ly6C^{low}$). Accordingly, MR antagonism upregulated the expression of some anti-inflammatory factors while downregulating the expression of proinflammatory cytokines in wound tissues. This is consistent with previous findings that showed the role of MR activation in various diseases involving chronic inflammation, including diabetes (Guo et al., 2008; Jaisser and Farman, 2015; Marzolla et al., 2014). Previous studies reported a central role of MR overactivation in sustained macrophage polarization after renal injury induced by ischemia-reperfusion (Barrera-Chimal et al., 2018). In this setting, pharmacological MR antagonism also promoted the polarization of activated M1 macrophages toward an anti-inflammatory M2 phenotype, suggesting that this may be a common mode of action of MR antagonists in wound healing in cardiovascular, renal, or metabolic injury (Barrera-Chimal et al., 2018).

Defective angiogenesis often occurs in diabetic wounds. The defect of wound angiogenesis may be because of inadequate mobilization and abnormal activation of endothelial progenitor cells (Loomans et al., 2004). Several therapies based on promoting the functional activity of endothelial cells and their progenitors have been proposed to improve healing (Liu et al., 2014; Marrotte et al., 2010; Nishimura et al., 2012). Impaired angiogenesis may also be associated with chronic inflammation, inhibiting the production of proangiogenic factors and limiting endothelial cell activity. Macrophages are important sources of proangiogenic factors. These inflammatory cells have been shown to be involved in many disease settings, including the complications of diabetes (Maruyama et al., 2007; Okizaki et al., 2015). Here, we found that M2 polarized macrophages, induced by the inhibition of MR signaling, expressed higher levels of proangiogenic factors than those from nontreated diabetic wounds, contributing to angiogenesis and wound healing improvement.

Overall, our results suggest an important role for MR signaling in the sustained polarization of macrophages and impaired wound angiogenesis in diabetes. These findings provide further insight concerning the impact of MR activation in various skin diseases. We previously reported the role of cutaneous MR overactivation in the deleterious effects caused by dermoglucocorticoid treatment in both mice and humans, including skin atrophy and impaired wound healing; GC-induced MR activation impaired the proliferation and activation of epidermal keratinocytes linked to overactivation of epithelial sodium channels. Topical cutaneous treatment with MR antagonists provided significant benefits, limiting atrophy and improving wound healing (Maubec et al., 2015; Nguyen et al., 2016). MR overexpression in keratinocytes was shown to induce epidermal atrophy in mice (Sainte Marie et al., 2007). Boix et al.(2016) demonstrated that epidermal deletion of MRs leads to increased keratinocyte proliferation and differentiation . Other studies proposed that epidermal MR cooperates with GC receptors, acting as an anti-inflammatory factor to counteract skin inflammation and regulate epidermal development in inflamed skin (Bigas et al., 2018; Sevilla and Pérez, 2018).

The mechanism underlying the modulation of inflammation and angiogenesis by MR in diabetic wounds may be complex and multifactorial. We identified LCN2, a primary target of aldosterone and MR signaling (Buonafine et al., 2018), as a promising candidate in diabetes-associated delayed wound healing. LCN2 secretion is increased in the wound lysates of diabetic foot ulcers because of the release of neutrophil extracellular traps (Fadini et al., 2019). LCN2 activation is also considered to be a biomarker for chronic inflammatory diseases of the skin, such as psoriasis and venous ulcers (Serra et al., 2013; Shao et al., 2016). In this study, wounds from diabetic *Lcn2*-KO mice had lower inflammation scores, with a lower ratio of M1 to M2 macrophages, increased angiogenesis, and better wound healing than those from wild-type mice with STZ injection. The role of LCN2 in the regulation of inflammation is complex. Cheng et al.(2015) demonstrated that LCN2 promotes M1 macrophage polarization after cardiac ischemia-reperfusion injury. In contrast, Guo et al.(2014) reported that LCN2-deficient mice displayed upregulation of M1 macrophage markers and downregulation of M2 markers in the adipose tissue and liver of mice fed a high-fat diet. In another setting, Warszawska et al.(2013) identified LCN2 as both a marker of deactivated macrophages and a macrophage deactivator in the lungs of mice with bacterial pneumonia. In this study, LCN2 inactivation had a positive effect on diabetic wounds, whereas it did not affect the healing of nondiabetic normal

mice. Our in vitro study on the function and polarization of macrophages showed a direct effect of recombinant LCN2 protein to prevent the switching of preactivated M1 macrophages to the M2 phenotype, although a limit of our approach is the use of macrophages isolated from the peritoneum rather than from the skin.

Other factors may influence diabetic wound healing. Abnormalities in hair follicles result in defective hair development and cycling, representing a sign of vascular impairment and organ damage in diabetic patients (Miranda et al., 2016). Efficiency of wound repair is also influenced by the hair follicle cycle; wound healing was found to be accelerated when mice are wounded in the late anagen stage, with enhanced re-epithelialization and angiogenesis and decreased immune cell infiltration (Ansell et al., 2011). Thus, it is crucial that control and experimental mice are in a comparable stage of hair follicle cycling for adequate comparison. Our diabetic mice and their respective controls are in telogen stage (see Materials and Methods), thus providing adequate comparison conditions.

The hair follicle expresses the MR (Jaisser and Farman, 2015), but limited knowledge is available on the direct effects of MR signaling and its blockade in hair biology. Postnatal overexpression of MR in epidermal mouse skin induced major hair follicle dystrophy leading to alopecia (Farman et al., 2010; Sainte Marie et al., 2007). However, epidermal MR deletion showed no impact on hair follicle number and cycling in normal adult skin (Sevilla and Pérez, 2018). We cannot rule out that, in diabetes, MR antagonism may affect hair cycle with a subsequent impact on wound healing. Future studies are required to investigate the relationship between MR overactivation, its blockade by canrenoate, and the abnormalities of hair follicles on wound repair and epidermal barrier function in diabetic skin. In the dermis, effects of MR antagonism on elastin and collagen synthesis and tissue remodeling after injuries have been reported (Mitts et al., 2010). Interestingly, it has been highlighted that MR plays a significant role in modulating collagen synthesis in various organs (Jaisser and Farman, 2015). Improvement of the defective dermal remodeling processes in diabetic wounds would represent important progress.

In summary, we identified a significant role of MR signaling in inflammation and impaired vascular density accompanying delayed diabetic wound healing using mouse models. This study indicates the efficacy of MR blockade to restore impaired re-epithelialization and angiogenesis and to reduce inflammation after an acute wound in diabetic mice; whether these benefits extend to human chronic diabetic wounds as leg ulcers remains to be demonstrated. In a previous report, we showed that application of a topical MR antagonist was safe and effective in healthy volunteers with dermocorticoid-associated skin atrophy and delayed wound healing (Maubec et al., 2015; Nguyen et al., 2016). Topical MR antagonism thus may be a simple and useful therapeutic strategy, providing a significant benefit to diabetic patients with delayed wound healing.

MATERIALS AND METHODS

Detailed information is provided in Supplementary Materials and Methods.

Wound healing in vivo

Two mouse models of diabetes were used for studying wound healing in vivo, STZ-induced type 1 diabetes and type 2 diabetes (db-db mice), with their appropriate controls. Wounds were generated with a 6-mm biopsy punch. For the db-db groups, wounds were done at 10 weeks of age. At that time, all the dorsum skin displayed a homogenous pink color. For the STZ groups, diabetes was induced at 10 weeks, and we performed wounds at 15 weeks of age. We have given a special attention to select dorsum areas at a telogen stage, featured by pink skin color after hair clipping. The histology of the lateral skin surrounding the healing wounds in both models confirmed our clinical evaluation because we could not find any evidence of anagen hair follicles (Supplementary Figure S6). MR blockade over the wound was achieved by local application of the MR antagonist potassium canrenoate or phosphate buffered saline, and wounds were photographed to evaluate wound closure. At day 5 (STZ groups) or 7 (db-db groups), mice were euthanized, and wound and skin specimens were collected for RNA and protein extraction, immunolabeling, or FACS analysis.

Diabetes was also induced by STZ injections in 10-week-old female *Lcn2*-KO mice (Berger et al., 2006) and their appropriate controls before wounding.

Local MR silencing by siRNA in wounds of diabetic type 1 mouse model

Mouse MR Stealth RNAi siRNAs (set of 3, MSS201383, MSS201384, and MSS272869) were purchased from Thermo Fisher Scientific (Waltham, MA). Stock solution was made by adding 1 ml water to 20 nmol MR siRNA set. The siRNA working solution was prepared by 1:10 dilution of siRNA stock solution with Mirus Transfection Reagent (Thermo Fisher Scientific). After wounding, 100 µl of siRNA solution (0.2 nmol) was locally injected with a needle into each wound at day 0 and day 2. The scrambled siRNA (Stealth RNAi negative control, medium GC duplex, Thermo Fisher Scientific) was prepared according to manufacturer's instruction and used as negative control. Photographs of wounds at day 3 and day 5 were used to evaluate the degree of wound closure. Mice were killed at day 5, and wounded skin samples were collected for histological and molecular analysis.

Animal study approval statement

All animal experiments were approved by the Darwin ethics committee of Pierre et Marie Curie University and the French Ministry of Research (APAFIS#4438-2015092514508030 v7) and in accordance with the INSERM guidelines and European Community directives for the care and use of laboratory animals.

Data availability statement

There are no datasets related to this article.

CONFLICT OF INTEREST

The authors state no conflict of interest.

ACKNOWLEDGMENTS

The authors are grateful for the excellent technical assistance of the CEF (animal facility) team and their support with the animal care. The authors are also grateful to Thorsten Berger and Tak W. Mak (University of Toronto, Canada) for kindly sharing the *Lcn2* KO mice. The authors are grateful to the following individuals for providing regular scientific advice and help: Sylvie Dumont and Fatiha Merabtene (Histo-morphology Platform, Saint-Antoine Research Center), Hélène Fohrer-Ting, Estelle Devevre, and Christophe Klein (Cellular Imaging and Cytometry Center, Cordeliers Research Center). This work was supported by INSERM funding, the Agence Nationale pour la Recherche (ANR-14-CE16-0010-01) and SATT INNOV maturation grant 494. VT Nguyen was a recipient of a PhD grant from the Vietnamese Government

and a grant from the Fondation pour la Recherche Médicale (grant FDT20140930932).

AUTHOR CONTRIBUTIONS

Conceptualization: NF, SA, FJ; Data Curation: VTN, NF, SA, FJ; Formal Analysis: VTN; Funding Acquisition: NF, FBC, SA, FJ; Investigation: VTN, MS, RPR; Methodology: VTN, NF, SA, FJ; Project Administration: NF, SA, FJ; Resources: FBC, SA, FJ; Supervision: NF, SA, FJ; Visualization: VTN, RPR; Writing - Original Draft Preparation: VTN, NF, SA, FJ; Writing - Review and Editing: VTN, NF, RPR, MS, FBC, SA, FJ.

SUPPLEMENTARY MATERIAL

Supplementary material is linked to the online version of the paper at www.jidonline.org, and at https://doi.org/10.1016/j.jid.2019.04.030.

REFERENCES

Ahmed AS, Antonsen EL. Immune and vascular dysfunction in diabetic wound healing. J Wound Care 2016;25(Suppl. 7):S35–46.

Ansell DM, Kloepper JE, Thomason HA, Paus R, Hardman MJ. Exploring the "hair growth–wound healing connection": anagen phase promotes wound re-epithelialization. J Invest Dermatol 2011;131:518–28.

Ashcroft GS, Jeong MJ, Ashworth JJ, Hardman M, Jin W, Moutsopoulos N, et al. Tumor necrosis factor-alpha (TNF-α) is a therapeutic target for impaired cutaneous wound healing. Wound Repair Regen 2012;20:38–49.

Barrera-Chimal J, Estrela GR, Lechner SM, Giraud S, El Moghrabi S, Kaaki S, et al. The myeloid mineralocorticoid receptor controls inflammatory and fibrotic responses after renal injury via macrophage interleukin-4 receptor signaling. Kidney Int 2018;93:1344–55.

Barrientos S, Stojadinovic O, Golinko MS, Brem H, Tomic-Canic M. PERSPECTIVE ARTICLE: Growth factors and cytokines in wound healing. Wound Repair Regen 2008;16:585–601.

Berger T, Togawa A, Duncan GS, Elia AJ, You-Ten A, Wakeham A, et al. Lipocalin 2-deficient mice exhibit increased sensitivity to Escherichia coli infection but not to ischemia-reperfusion injury. Proc Natl Acad Sci USA 2006;103:1834–9.

Bigas J, Sevilla LM, Carceller E, Boix J, Pérez P. Epidermal glucocorticoid and mineralocorticoid receptors act cooperatively to regulate epidermal development and counteract skin inflammation. Cell Death Dis 2018;9:588.

Boix J, Sevilla LM, Sáez Z, Carceller E, Pérez P. Epidermal mineralocorticoid receptor plays beneficial and adverse effects in skin and mediates glucocorticoid responses. J Invest Dermatol 2016;136:2417–26.

Boniakowski AE, Kimball AS, Jacobs BN, Kunkel SL, Gallagher KA. Macrophage-mediated inflammation in normal and diabetic wound healing. J Immunol 2017;199:17–24.

Boulton AJ, Vileikyte L, Ragnarson-Tennvall G, Apelqvist J. The global burden of diabetic foot disease. Lancet 2005;366:1719–24.

Boulton AJM. Diabetic neuropathy and foot complications. Handb Clin Neurol 2014;126:97–107.

Brancato SK, Albina JE. Wound macrophages as key regulators of repair. Am J Pathol 2011;178:19–25.

Brem H, Tomic-Canic M. Cellular and molecular basis of wound healing in diabetes. J Clin Invest 2007;117:1219–22.

Buonafine M, Martinez-Martinez E, Jaisser F. More than a simple biomarker: the role of NGAL in cardiovascular and renal diseases. Clin Sci 2018;132:909–23.

Cheng L, Xing H, Mao X, Li L, Li X, Li Q. Lipocalin-2 promotes m1 macrophages polarization in a mouse cardiac ischaemia-reperfusion injury model. Scand J Immunol 2015;81:31–8.

Clokie M, Greenway AL, Harding K, Jones NJ, Vedhara K, Game F, et al. New horizons in the understanding of the causes and management of diabetic foot disease: report from the 2017 Diabetes UK Annual Professional Conference Symposium. Diabet Med 2017;34:305–15.

Dinh T, Tecilazich F, Kafanas A, Doupis J, Gnardellis C, Leal E, et al. Mechanisms involved in the development and healing of diabetic foot ulceration. Diabetes 2012;61:2937–47.

Fadini GP, Solini A, Manca ML, Penno G, Gatti A, Anichini R, et al. Effectiveness of dapagliflozin versus comparators on renal endpoints in the real world: A multicentre retrospective study. Diabetes Obes Metab 2019;21:252–60.

Farman N, Maubec E, Poeggeler B, Klatte JE, Jaisser F, Paus R. The mineralocorticoid receptor as a novel player in skin biology: beyond the renal horizon? Exp Dermatol 2010;19:100–7.

Galiano RD, Tepper OM, Pelo CR, Bhatt KA, Callaghan M, Bastidas N, et al. Topical vascular endothelial growth factor accelerates diabetic wound healing through increased angiogenesis and by mobilizing and recruiting bone marrow-derived cells. Am J Pathol 2004;164:1935–47.

Gordon S. Alternative activation of macrophages. Nat Rev Immunol 2003;3:23–35.

Greenhalgh DG. Wound healing and diabetes mellitus. Clin Plast Surg 2003;30:37–45.

Guo C, Ricchiuti V, Lian BQ, Yao TM, Coutinho P, Romero JR, et al. Mineralocorticoid receptor blockade reverses obesity-related changes in expression of adiponectin, peroxisome proliferator-activated receptor-γ, and proinflammatory adipokines. Circulation 2008;117:2253–61.

Guo H, Jin D, Chen X. Lipocalin 2 is a regulator of macrophage polarization and NF-κB/STAT3 pathway activation. Mol Endocrinol 2014;28:1616–28.

Guo Y, Lin C, Xu P, Wu S, Fu X, Xia W, et al. AGEs induced autophagy impairs cutaneous wound healing via stimulating macrophage polarization to M1 in diabetes. Sci Rep 2016;6:36416.

Hannen R, Udeh-Momoh C, Upton J, Wright M, Michael A, Gulati A, et al. Dysfunctional skin-derived glucocorticoid synthesis is a pathogenic mechanism of psoriasis. J Invest Dermatol 2017;137:1630–7.

He R, Yin H, Yuan B, Liu T, Luo L, Huang P, et al. IL-33 improves wound healing through enhanced M2 macrophage polarization in diabetic mice. Mol Immunol 2017;90:42–9.

Hirata A, Maeda N, Hiuge A, Hibuse T, Fujita K, Okada T, et al. Blockade of mineralocorticoid receptor reverses adipocyte dysfunction and insulin resistance in obese mice. Cardiovasc Res 2009;84:164–72.

Jaisser F, Farman N. Emerging roles of the mineralocorticoid receptor in pathology: toward new paradigms in Clinical Pharmacology. Pharmacol Rev 2015;68:49–75.

Leal EC, Carvalho E, Tellechea A, Kafanas A, Tecilazich F, Kearney C, et al. Substance P promotes wound healing in diabetes by modulating inflammation and macrophage phenotype. Am J Pathol 2015;185:1638–48.

Lepantalo M, Apelqvist J, Setacci C, Ricco JB, de Donato G, Becker F, et al. Chapter V: Diabetic foot. Eur J Vasc Endovasc Surg 2011;42(Suppl. 2):S60–74.

Liu F, Chen DD, Sun X, Xie HH, Yuan H, Jia W, et al. Hydrogen sulfide improves wound healing via restoration of endothelial progenitor cell functions and activation of angiopoietin-1 in type 2 diabetes. Diabetes 2014;63:1763–78.

Loomans CJM, de Koning EJP, Staal FJT, Rookmaaker MB, Verseyden C, de Boer HC, et al. Endothelial progenitor cell dysfunction: a novel concept in the pathogenesis of vascular complications of type 1 diabetes. Diabetes 2004;53:195–9.

Lucas T, Waisman A, Ranjan R, Roes J, Krieg T, Müller W, et al. Differential roles of macrophages in diverse phases of skin repair. J Immunol 2010;184:3964–77.

Mahdavian Delavary B, van der Veer WM, van Egmond M, Niessen FB, Beelen RHJ. Macrophages in skin injury and repair. Immunobiology 2011;216:753–62.

Mantovani A, Sica A, Sozzani S, Allavena P, Vecchi A, Locati M. The chemokine system in diverse forms of macrophage activation and polarization. Trends Immunol 2004;25:677–86.

Marrotte EJ, Chen DD, Hakim JS, Chen AF. Manganese superoxide dismutase expression in endothelial progenitor cells accelerates wound healing in diabetic mice. J Clin Invest 2010;120:4207–19.

Martínez-Martínez E, Buonafine M, Boukhalfa I, Ibarrola J, Fernández-Celis A, Kolkhof P, et al. Aldosterone target NGAL (neutrophil gelatinase–associated lipocalin) is involved in cardiac remodeling after myocardial infarction through NFκB pathway. Hypertension 2017;70:1148–56.

Maruyama K, Asai J, Ii M, Thorne T, Losordo DW, D'Amore PA. Decreased macrophage number and activation lead to reduced lymphatic vessel formation and contribute to impaired diabetic wound healing. Am J Pathol 2007;170:1178–91.

Marzolla V, Armani A, Feraco A, De Martino MU, Fabbri A, Rosano G, et al. Mineralocorticoid receptor in adipocytes and macrophages: a promising target to fight metabolic syndrome. Steroids 2014;91:46–53.

Maubec E, Laouénan C, Deschamps L, Nguyen VT, Scheer-Senyarich I, Wackenheim-Jacobs AC, et al. Topical mineralocorticoid receptor blockade limits glucocorticoid-induced epidermal atrophy in human skin. J Invest Dermatol 2015;135:1781–9.

Miranda JJ, Taype-Rondan A, Tapia JC, Gastanadui-Gonzalez MG, Roman-Carpio R. Hair follicle characteristics as early marker of Type 2 Diabetes. Med Hypo 2016;95:39–44.

Mitts TF, Bunda S, Wang Y, Hinek A. Aldosterone and mineralocorticoid receptor antagonists modulate elastin and collagen deposition in human skin. J Invest Dermatol 2010;130:2396–406.

Nguyen VT, Farman N, Maubec E, Nassar D, Desposito D, Waeckel L, et al. Re-epithelialization of pathological cutaneous wounds is improved by local mineralocorticoid receptor antagonism. J Invest Dermatol 2016;136:2080–9.

Nishimura Y, Ii M, Qin G, Hamada H, Asai J, Takenaka H, et al. CXCR4 antagonist AMD3100 accelerates impaired wound healing in diabetic mice. J Invest Dermatol 2012;132(3 Pt 1):711–20.

Noor S, Khan RU, Ahmad J. Understanding diabetic foot infection and its management. Diabetes Metab Syndr 2017;11:149–56.

Novak ML, Koh TJ. Phenotypic transitions of macrophages orchestrate tissue repair. Am J Pathol 2013;183:1352–63.

Okizaki S, Ito Y, Hosono K, Oba K, Ohkubo H, Amano H, et al. Suppressed recruitment of alternatively activated macrophages reduces TGF-beta1 and impairs wound healing in streptozotocin-induced diabetic mice. Biomed Pharmacother 2015;70:317–25.

Peters EJG, Lipsky BA. Diagnosis and management of infection in the diabetic foot. Med Clin North Am 2013;97:911–46.

Rahmani W, Liu Y, Rosin NL, Kline A, Raharjo E, Yoon J, et al. Macrophages promote wound-induced hair follicle regeneration in a CX3CR1- and TGF-β1–Dependent manner. J Invest Dermatol 2018;138:2111–22.

Ramalho T, Filgueiras L, Silva-Jr IA, Pessoa AFM, Jancar S. Impaired wound healing in type 1 diabetes is dependent on 5-lipoxygenase products. Sci Rep 2018;8:14164.

Sainte Marie Y, Toulon A, Paus R, Maubec E, Cherfa A, Grossin M, et al. Targeted skin overexpression of the mineralocorticoid receptor in mice causes epidermal atrophy, premature skin barrier formation, eye abnormalities, and alopecia. Am J Pathol 2007;171:846–60.

Serra R, Buffone G, Falcone D, Molinari V, Scaramuzzino M, Gallelli L, et al. Chronic venous leg ulcers are associated with high levels of metalloproteinases-9 and neutrophil gelatinase-associated lipocalin. Wound Repair Regen 2013;21:395–401.

Sevilla LM, Pérez P. Roles of the glucocorticoid and mineralocorticoid receptors in skin pathophysiology. Int J Mol Sci 2018;19:E1906.

Shao S, Cao T, Jin L, Li B, Fang H, Zhang J, et al. Increased Lipocalin-2 contributes to the pathogenesis of psoriasis by modulating neutrophil chemotaxis and cytokine secretion. J Invest Dermatol 2016;136:1418–28.

Sindrilaru A, Peters T, Wieschalka S, Baican C, Baican A, Peter H, et al. An unrestrained proinflammatory M1 macrophage population induced by iron impairs wound healing in humans and mice. J Clin Invest 2011;121:985–97.

Slominski AT, Manna PR, Tuckey RC. Cutaneous glucocorticosteroidogenesis: securing local homeostasis and the skin integrity. Exp Dermatol 2014;23:369–74.

Slominski AT, Manna PR, Tuckey RC. On the role of skin in the regulation of local and systemic steroidogenic activities. Steroids 2015;103:72–88.

Stojadinovic O, Lindley LE, Jozic I, Tomic-Canic M. Mineralocorticoid receptor antagonists—A new sprinkle of salt and youth. J Invest Dermatol 2016;136:1938–41.

Tiganescu A, Tahrani AA, Morgan SA, Otranto M, Desmoulière A, Abrahams L, et al. 11beta-Hydroxysteroid dehydrogenase blockade prevents age-induced skin structure and function defects. J Clin Invest 2013;123:3051–60.

Warszawska JM, Gawish R, Sharif O, Sigel S, Doninger B, Lakovits K, et al. Lipocalin 2 deactivates macrophages and worsens pneumococcal pneumonia outcomes. J Clin Invest 2013;123:3363–72.

Zhang P, Lu J, Jing Y, Tang S, Zhu D, Bi Y. Global epidemiology of diabetic foot ulceration: a systematic review and meta-analysis. Ann Med 2017;49:106–16.

SUPPLEMENTARY MATERIALS AND METHODS

Reagents and antibodies

Reagents and drugs were purchased from Sigma-Aldrich (St. Louis, MO) unless specified. Culture medium was purchased from Gibco (Life Technologies, Carlsbad, CA). Recombinant mouse LCN2 protein was purchased from R&D Systems (Minneapolis, MN).

The following antibodies were used for immunohistochemistry and immunofluorescence staining: rabbit polyclonal anti-keratin 14 (Covance, Princeton, NJ); rabbit polyclonal anti-Ki67 and rabbit polyclonal anti-CD31 (Abcam, Cambridge, United Kingdom); and rat anti-mouse CD31 (Biolegend, San Diego, CA). The following antibodies were used for flow cytometry analysis: PE/Cy7-conjugated rat anti-F4/80, FITC-conjugated rat anti-CD31, APC-conjugated rat anti-CD45, APC/Cy7-conjugated rat anti-CD11b, PE-conjugated rat anti-Ly6C, and FITC-conjugated rat anti-CD206 (Biolegend).

Animals

All experiments were performed using 10- to 15-week-old female mice (Janvier Laboratories, Le Genest-Saint-Isle, France). Type 1 diabetes was induced in 10-week-old C57BL/6j mice by daily intraperitoneal injection of streptozotocin (STZ; 50 g/kg) in 0.05 mol/L citrate buffer (pH 4.5) for 5 days. Citrate buffer–injected mice were used as controls. Blood glucose levels were measured using the OneTouch Vita Kit (LifeScan, Milpitas, CA) 4 weeks after STZ treatment. Animals with blood glucose levels $>$ 350 mg/dl were considered to be diabetic and were used for subsequent experiments. Ten-week-old db-db mice were used as a model for type 2 diabetes. Db/$^{+}$ mice served as controls. Female C57BL/6j *Lcn2* whole-body knockout (Berger et al., 2006) and wild-type littermate controls were generated through appropriate breeding at our animal facility.

Wounds were generated using a 6-mm biopsy punch; MR blockade over the wound was achieved by local application of the MR antagonist potassium canrenoate (0.5 mM) or phosphate buffered saline, and the wounds were photographed to evaluate the degree of wound closure. At day 5 (STZ) or 7 (db-db), mice were euthanized and wound and skin specimens collected.

Primary murine macrophage culture

Macrophages were collected from the peritoneum by lavage 5 days after a single intraperitoneal injection of 3 ml of 3% thioglycolate medium. The cells were then plated in RPMI 1640 media containing 10% fetal bovine serum and 1% penicillin-streptomycin and incubated for 1 day in an incubator at 37 °C and 5% CO_2, followed by 24 hours of stimulation with 100 ng/ml lipopolysaccharide to promote the M1 phenotype. M1 macrophages were then switched to M2 phenotype by 10 ng/ml IL-4 in the presence or absence of recombinant mouse LCN2 protein (1.5 μg/ml) for 48 hours (Supplementary Figure S4a). Cells were harvested and processed for FACS analysis or RNA extraction.

FACS analysis

Cell suspensions isolated from wounded tissue harvested at day 5 or 7 after wounding or in vitro cultured macrophages were used for FACS analysis, according to established methods with minor modifications (Adamson et al., 2016; Nassar et al., 2012). Briefly, 1×10^6 cells were suspended in 1% fetal bovine serum/phosphate buffered saline and incubated with a combination of fluorescence-conjugated antibodies in the dark for 1 hour at 4 °C. FACS data were acquired using a BD LSR II cytometer (BD Pharmingen, San Diego, CA) and analyzed using FlowJo software (TreeStar Inc, Ashland, OR). Various cell populations were calculated as the percentage of total living cells. Specific marker expression is given as the geometric mean of conjugated fluorescence intensity. Wound macrophages were sorted using an Influx Flow cytometer (BD Pharmingen).

LCN2 protein detection by ELISA

Total LCN2 protein from the wounds was assessed using a DuoSet ELISA kit (R&D Systems), according to the manufacturer's instructions. Briefly, 100 μl (3.5 μg protein) of each sample were applied to a 96-well plate previously coated with rat anti-mouse LCN2 capture antibody (Vitro, Madrid, Spain) and blocked for 2 hours. After washing, biotinylated rat anti-mouse LCN2 detection antibody was added and the plate incubated for 2 hours. HRP-conjugated streptavidin was then added and the plate incubated for an additional 20 minutes. Finally, substrate solution was added, the plate incubated for 20 minutes, and color development assessed by a microplate reader set to 450 nm.

Immunohistochemistry and immunofluorescence staining

Immunohistochemistry for CD31 was performed on sections (5 μm) from paraffin-embedded paraformaldehyde-fixed wound tissue of db-db mice using the Novolink Polymer Detection Systems kit from Leica Microsystems (Nanterre, France) following the protocol of the manufacturer. Immunofluorescence staining was performed on 6 μm cryosections (STZ mice) or 5 μm paraformaldehyde-fixed paraffin sections (db-db mice) as described (Nguyen et al., 2016). Ki67-labeled cells from 5 different fields were quantified as a percentage of DAPI-stained nuclei. The length of the newly formed epidermis was calculated by adding the lengths of the neoepithelial tongues on both sides of the wound from the tip of the epidermis to the site of the first hair follicle at the wound margin. The surface of CD31^{+} blood vessels (with open and closed lumen) was measured in 5 different fields on CD31-labeled sections, and the data are presented as a percentage of the total surface of the wound (Cho et al., 2006; Khosrotehrani et al., 2011; Michalczyk et al., 2018). Double stained Ki67/CD31 cells were used as an index of neovascularization in wounds.

Real-time PCR

Total RNA extraction and real-time PCR were performed as previously described (Maubec et al., 2015). The samples were assayed in triplicate. Gene expression was normalized to the relative levels of glucose-6-phosphate dehydrogenase (values in controls were set to 1 and those in the treated zones are expressed as fold changes). Primers were

purchased from Eurogentec (Liège, Belgium); the sequences of primers used in this study are shown in Supplementary Table S1.

Statistics

Statistical analyses were performed using GraphPad Prism software version 6.0. Results are expressed as mean ± standard error of the mean. Differences between the means of two groups were assessed using a nonparametric Mann-Whitney test. Differences between multiple groups were analyzed by one-way analysis of variance followed by the Newman-Keuls multiple comparison test. $P < 0.05$ was considered to be statistically significant.

SUPPLEMENTARY REFERENCES

Adamson SE, Griffiths R, Moravec R, Senthivinayagam S, Montgomery G, Chen W, et al. Disabled homolog 2 controls macrophage phenotypic polarization and adipose tissue inflammation. J Clin Invest 2016;126:1311–22.

Berger T, Togawa A, Duncan GS, Elia AJ, You-Ten A, Wakeham A, et al. Lipocalin 2-deficient mice exhibit increased sensitivity to Escherichia coli infection but not to ischemia-reperfusion injury. Proc Natl Acad Sci USA 2006;103:1834–9.

Cho C-H, Sung H-K, Kim K-T, Cheon HG, Oh GT, Hong HJ, et al. COMP-angiopoietin-1 promotes wound healing through enhanced angiogenesis, lymphangiogenesis, and blood flow in a diabetic mouse model. Proc Natl Acad Sci USA 2006;103:4946–51.

Khosrotehrani K, Huu SN, Prignon A, Avril MF, Boitier F, Oster M, et al. Pregnancy promotes melanoma metastasis through enhanced lymphangiogenesis. Am J Pathol 2011;178:1870–80.

Maubec E, Laouénan C, Deschamps L, Nguyen VT, Scheer-Senyarich I, Wackenheim-Jacobs AC, et al. Topical mineralocorticoid receptor blockade limits glucocorticoid-induced epidermal atrophy in human skin. J Invest Dermatol 2015;135:1781–9.

Michalczyk ER, Chen L, Fine D, Zhao Y, Mascarinas E, Grippo PJ, et al. Pigment epithelium-derived factor (PEDF) as a regulator of wound angiogenesis. Sci Rep 2018;8:11142.

Nassar D, Droitcourt C, Mathieu-d'Argent E, Kim MJ, Khosrotehrani K, Aractingi S. Fetal progenitor cells naturally transferred through pregnancy participate in inflammation and angiogenesis during wound healing. FASEB J 2012;26:149–57.

Nguyen VT, Nassar D, Batteux F, Raymond K, Tharaux PL, Aractingi S. Delayed healing of sickle cell ulcers is due to impaired angiogenesis and CXCL12 secretion in skin wounds. J Invest Dermatol 2016;136:497–506.

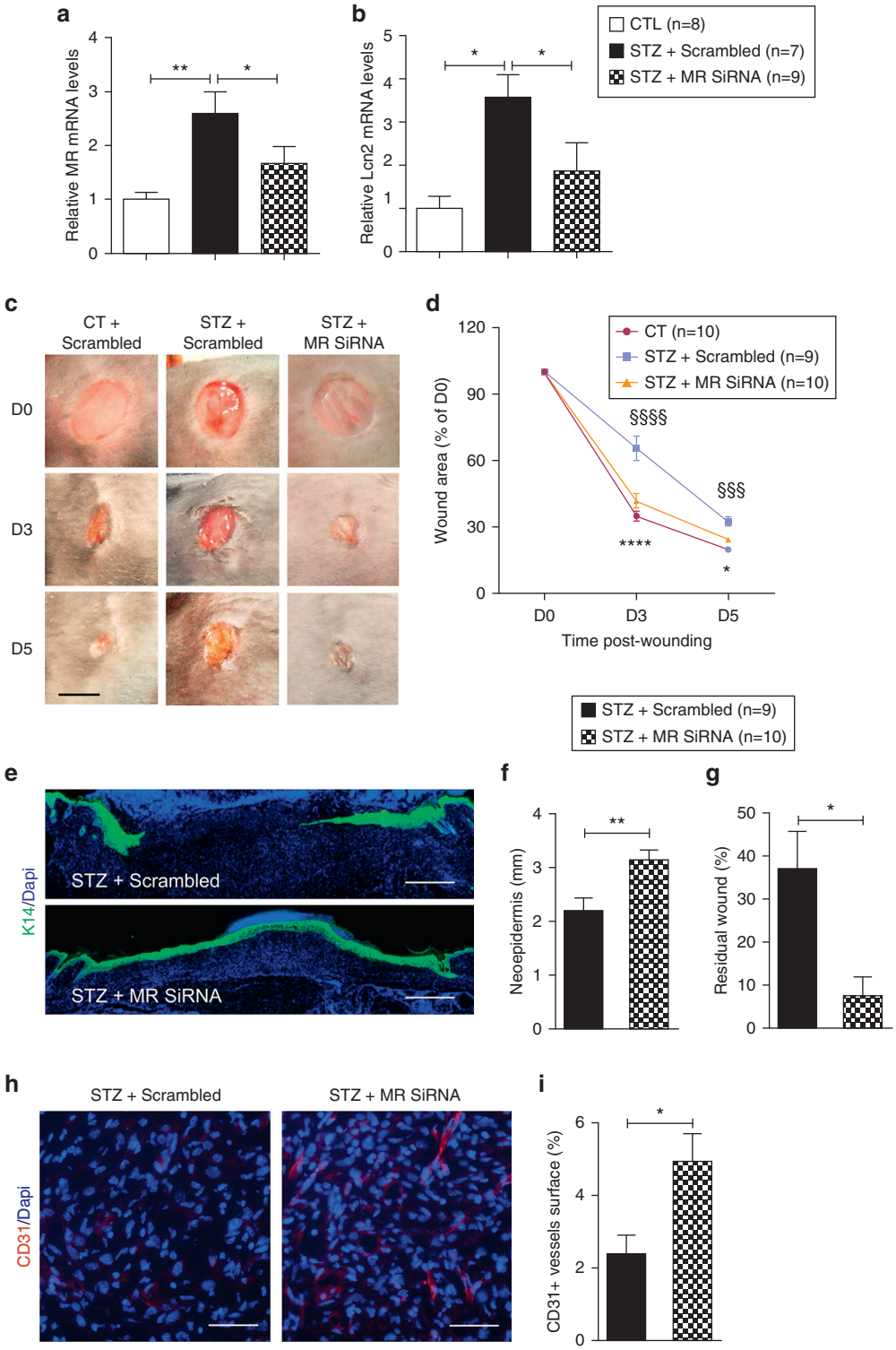

Supplementary Figure S1. MR siRNA improves the delayed wound healing in type 1 diabetic mice. Wounds of CT and STZ-injected mice were treated locally with MR siRNA or scrambled control siRNA at day 0 and day 2 post-wounding. Wounded skin was harvested at day 5 for analysis. mRNA levels of (**a**) MR and (**b**) LCN2 in wounds were analyzed by real-time PCR, relative to that of CT. (**c**) Photographs and (**d**) quantification of the wound area from CT and STZ mice with or without MR siRNA treatment at the indicated times post-wounding. (**e**) Wound sections at day 5 post-wounding labeled with anti-K14 antibody (green) and DAPI (blue). Quantification of (**f**) the length of the neoepidermis and (**g**) the size of the residual wound. (**h**) Photographs of wound sections stained for CD31, showing neomicrovessels formed in wound beds of STZ mice treated with MR siRNA or scrambled control and (**i**) quantification. Data represent mean ± SEM; n = number of mice per group, from 2 experimental series. (a, b) One-way ANOVA followed by the Newman-Keuls multiple comparison test; (d) Two-way ANOVA followed by the Newman-Keuls multiple comparison test. (f, g, i) Mann-Whitney test. $^{*}P < 0.05$; $^{**}P < 0.01$; $^{***}P < 0.001$; $^{****}P < 0.0001$, STZ vs CT.(d) §$P<0.05$, §§§§$P<0.0001$, STZ + MR siRNA vs STZ + scrambled siRNA. ANOVA, analysis of variance; CT, control; MR, mineralocorticoid receptor; siRNA, small interfering RNA; SEM, standard error of the mean; STZ, streptozotocin. Bar = 100 μm.

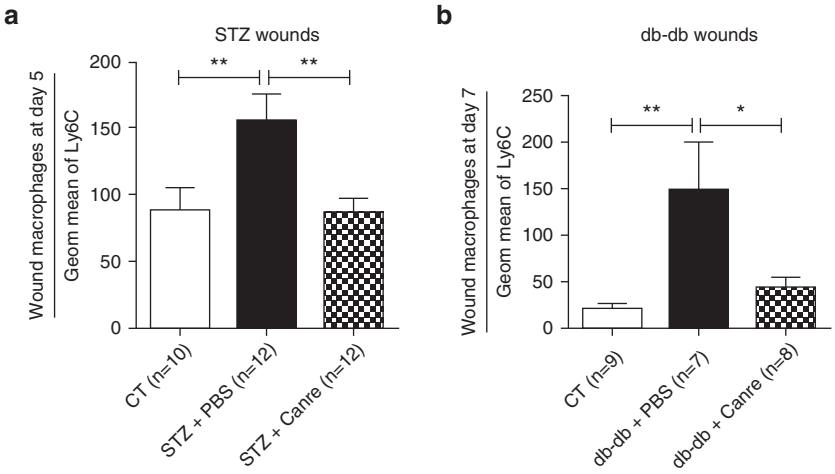

Supplementary Figure S2. Canrenoate prevents overexpression of M1 macrophage markers in diabetic wounds. Geometric mean fluorescence intensity of Ly6C (marker of M1 macrophages) was analyzed on macrophage populations from wounds of (**a**) db/db mice at day 7 and (**b**) STZ mice at day 5 post-wounding. Data represent mean ± SEM; n = number of mice per group, from 3 (STZ groups) and 2 (db-db groups) experimental series. One-way ANOVA followed by the Newman-Keuls multiple comparison test. $^{*}P < 0.05$; $^{**}P < 0.01$. ANOVA, analysis of variance; CT, control; PBS, phosphate buffered saline; SEM, standard error of the mean; STZ, streptozotocin.

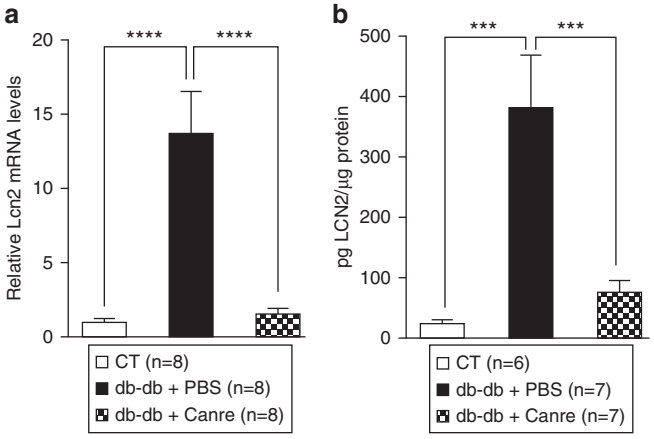

Supplementary Figure S3. Canrenoate normalizes the enhanced production of LCN2 in db-db wounds. (**a**) mRNA and (**b**) protein levels of LCN2 in wounds at day 7 were analyzed by real-time PCR and ELISA. Data represent mean ± SEM; n = number of mice per group, from 2 experimental series. One-way ANOVA followed by the Newman-Keuls multiple comparison test. $^{***}P < 0.001$; $^{****}P < 0.0001$. ANOVA, analysis of variance; CT, control; SEM, standard error of the mean.

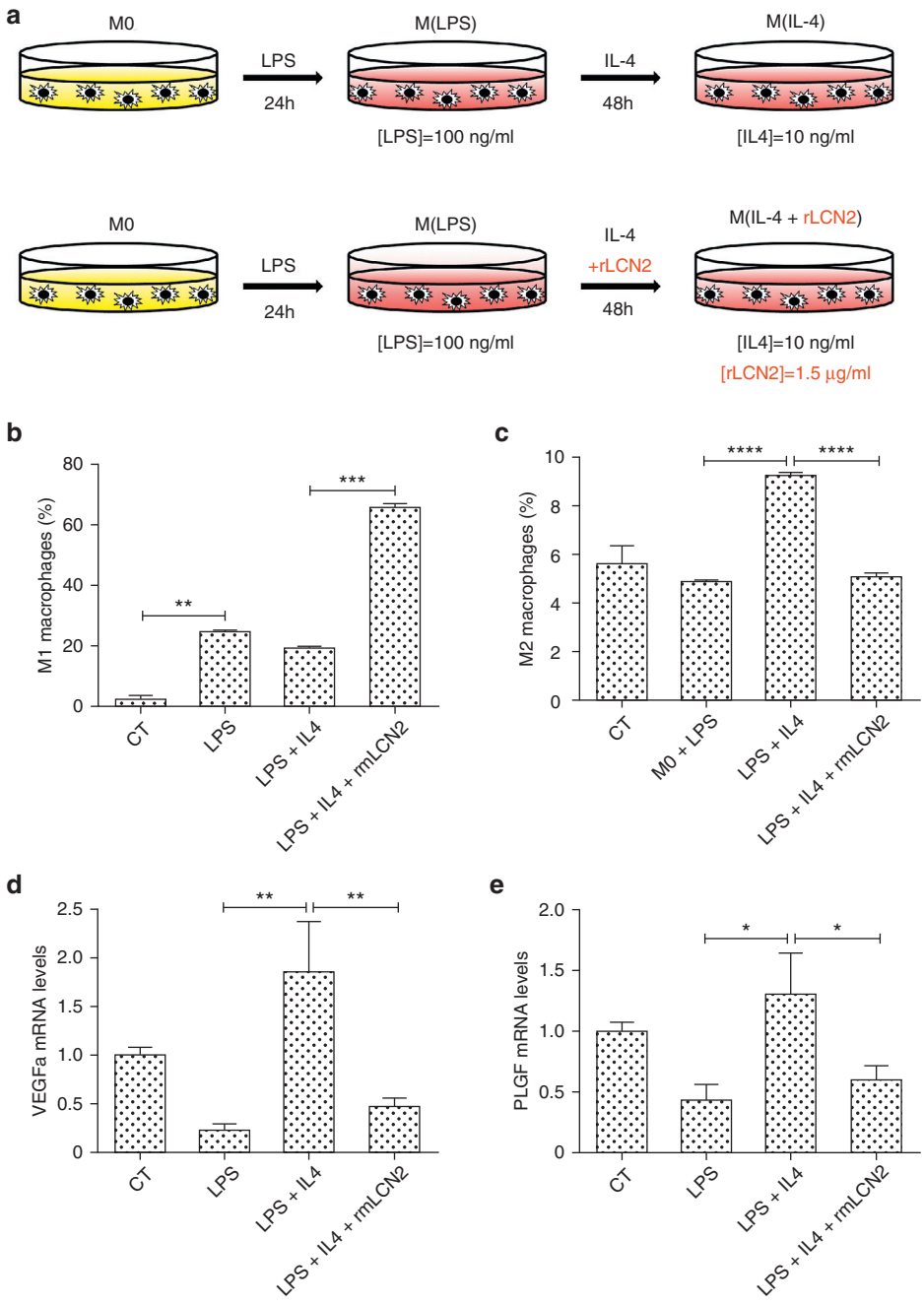

Supplementary Figure S4. Recombinant LCN2 protein prevents switching of M1 to M2 macrophages in vitro. (**a**) Peritoneal macrophages were collected from wild-type mice and cultured in RPMI medium followed by 24 hours of stimulation with 100 ng/ml LPS to promote M1 phenotype. M1 macrophages were then switched to M2 phenotype by 10 ng/ml IL-4 in the presence or absence of recombinant mouse LCN2 protein (1.5 µg/ml) for 48 hours. (**b**) M1 and (**c**) M2 macrophage populations were quantified by FACS analysis. Total RNA was extracted from cultured macrophages and the levels of angiogenic factors (**d**) *Vegfa* and (**e**) *Plgf* analyzed by qPCR. Data represent mean ± SEM, $n = 6$ for each condition. One-way ANOVA followed by the Newman-Keuls multiple comparison test. $^{*}P < 0.05$; $^{**}P < 0.01$; $^{***}P < 0.001$; $^{****}P < 0.0001$. ANOVA, analysis of variance; CT, control; LPS, lipopolysaccharide; qPCR, quantitative real-time reverse transcriptase–PCR; SEM, standard error of the mean.

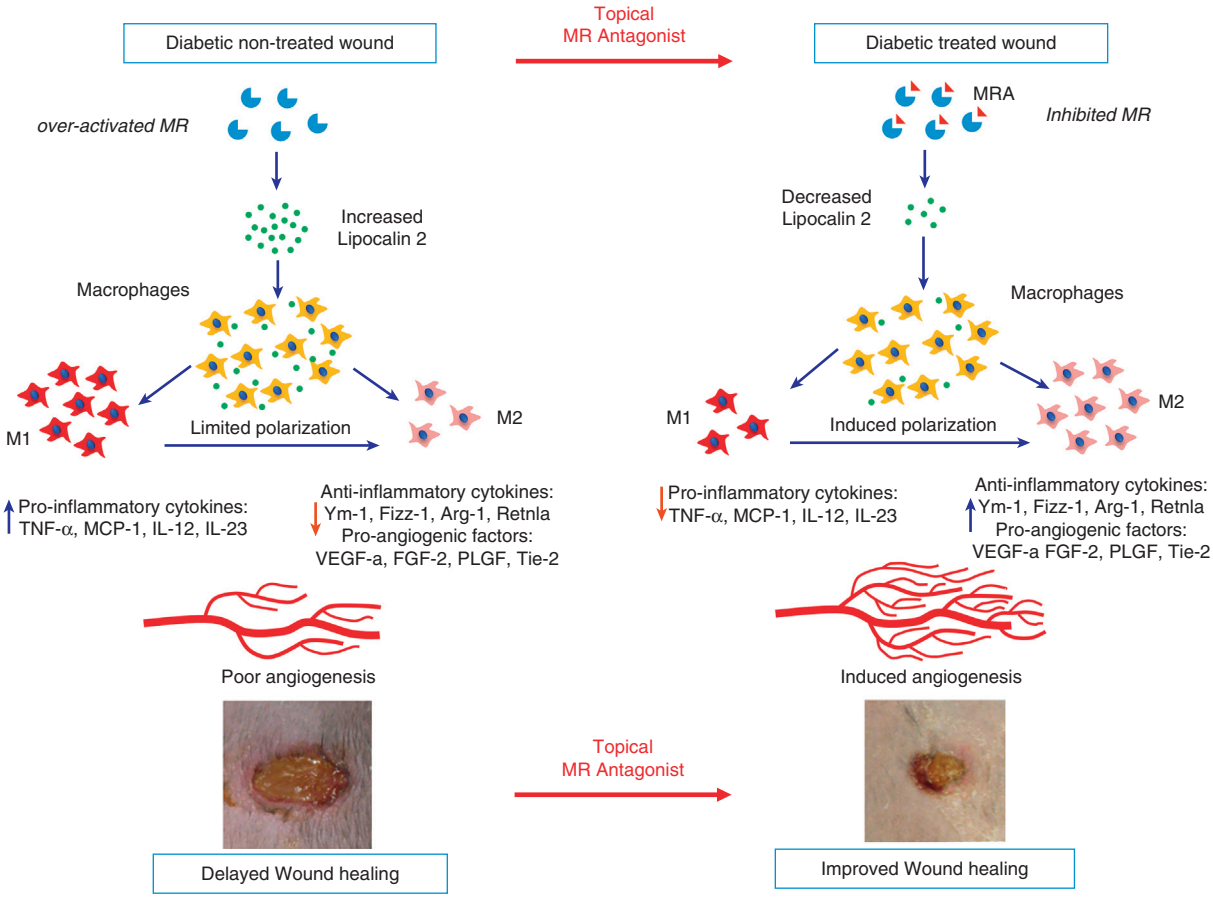

Supplementary Figure S5. Schematic model for effects of topical MR antagonist on delayed wound healing of diabetes. In diabetic wounds, enhanced MR signaling leads to increased secretion of LCN2. Topical MR antagonist limits the production of LCN2 in diabetic wounds, leading to a switch of macrophage polarization toward M2 phenotype. Induced M2 macrophage polarization results in (1) decreased expression of proinflammatory cytokines and increased expression of anti-inflammatory cytokines, therefore preventing prolonged inflammation of diabetic wounds, and (2) increased expression of angiogenic factors leading to increased angiogenesis and improved wound repair in diabetes. MR, mineralocorticoid receptor.

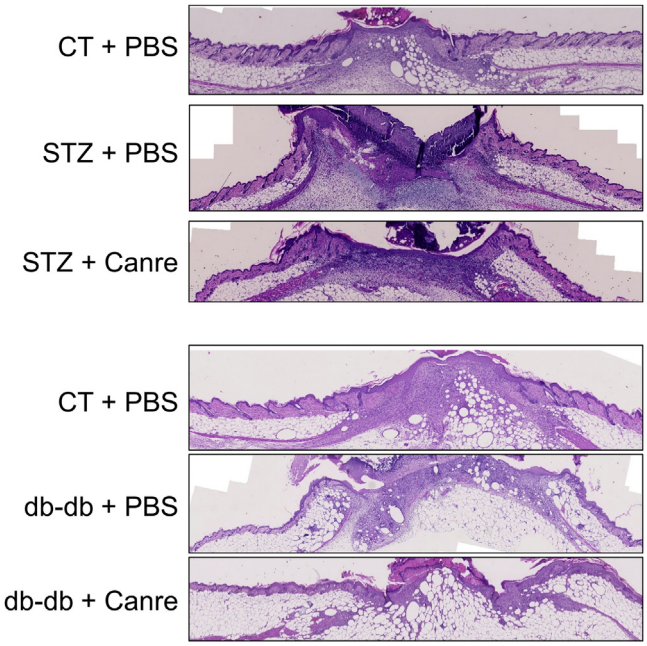

Supplementary Figure S6. Histology of wounded skin. H&E staining of wounded skin sections showing the histology of wounds and surrounding skin of mice from (**a**) STZ groups and (**b**) db-db groups. H&E, hematoxylin and eosin.

Supplementary Table S1. The sequences of quantitative RT-PCR primers

Gene	Forward	Reverse
Gapdh	GTGGCAAAGTGGAGATTGTTGCC	GATGATGACCCGTTTGGCTCC
Mr	CCAGAAGAGGGGACCACATA	GGAATTGTCGTAGCCTGCAT
Il6	CTCTGGGAAATCGTGGAAATG	AAGTGCATCATCGTTGTTCATACA
Tnfa	GCCTCTTCTCATTCCTGCTTG	CTGATGAGAGGGAGGCCATT
Mcp1	ATCCCAATGAGTAGGCTGGAGAGC	CAGAAGTGCTTGAGGTGGTTGTG
Il1b	CAAATCTCGCAGCAGCACA	TCATGTCCTCATCCTGGAAGG
Il12	GCCCTCTCTCTCCTCTTGCT	GTCTGCCTCTTTTGGTCAGG
Il23	CCAGCGGGACATATGAATCT	AGGCTCCCCTTTGAAGATGT
Ym1	GGGCATACCTTTATCCTGAG	CCACTGAAGTCATCCATGTC
Retnla	CCCTCCACTGTAACGAAGAC	CAACGAGTAAGCACAGGCAG
Il10	AGCCGGGAAGACAATAACTG	CATTTCCGATAAGGCTTGG
Fizz1	TCCCAGTGAATACTGATGAGA	CCACTCTGGATCTCCCAAGA
Arg1	CGCCTTTCTCAAAAGGACAG	CCAGCTCTTCATTGGCTTTC
Mmp9	CAGGAGTCTGGATAAGTTGG	CTGGAAGATGTCGTGTGAGT
Lcn2	CTACAATGTCACCTCCATCCTGG	GCATATTTCCCAGAGTGAACTGGC
Fgf2	CACCAGGCCACTTCAAGGAC	ATAGCAAGGTACCGGTTGGC
Plgf	TGCTGGGAACAACTCAACAGAA	TCTCCATGGGCCGACAGTAG
Vegfa	CAGGCTGCTGTAACGATGAA	AATGCTTTCTCCGCTCTGAA
Angpt1	CACGTGGAGCCGGATTTCT	ATCTGGGCCATCTCCGACTT
Angpt2	TAGCATCAGCCAACCAGGA	AAGGACCACATGCGTCAAAC
Tie2	ATGTGGAAGTCGAGAGGCGAT	CGAATAGCCATCCACTATTGTCC